

Fabrication and characterization of patterned micrometre scale interpenetrating Au–TiO₂ network nanocomposites

Abu Samah Zuruzi¹, Marcus S Ward¹ and Noel C MacDonald^{1,2}

¹ Materials Department, University of California, Santa Barbara, CA 93106, USA

² Mechanical and Environmental Engineering Department, University of California, Santa Barbara, CA 93106, USA

Received 30 January 2005, in final form 23 March 2005

Published 12 May 2005

Online at stacks.iop.org/Nano/16/1029

Abstract

Integrated micrometre scale interpenetrating Au–nanostructured TiO₂ (Au–NST) network nanocomposites have been fabricated using a two-step process. First, NST pad arrays were prepared by reacting patterned Ti surfaces with aqueous H₂O₂. NST formed is porous with pores 50–200 nm in diameter and walls about 75–125 nm thick. Second, Au was infiltrated into pores of NST using electroless deposition to form the nanocomposite. SEM studies indicate that Au was deposited into pores of NST with little void formation. Selective deposition of Au on NST pads was confirmed using XRD and area-mode XPS. This process is a general route to forming micrometre-scale nanocomposite features consisting of NST and metals that are amenable to electroless deposition.

(Some figures in this article are in colour only in the electronic version)

1. Introduction

Nanocomposites are materials in which at least one of the phases has constituents less than 100 nm in size [1]. Currently, thin films of metal–ceramic nanocomposites attract tremendous attention due to their fascinating properties and diverse potential for applications in electronics, optoelectronics, magnetics and catalysis [2]. Methods for fabricating metal–ceramic nanocomposites include evaporation [3, 4], sputtering [5, 6] and sol–gel processing [7–12]. Among these, the sol–gel process has received tremendous attention as it renders molecular-level control, is relatively low cost and allows the incorporation of various metal dopants into ceramic matrices. Conventional sol–gel processing, generally, results in a continuous gel film on a surface. In applications where patterned features are required, additional steps are employed such as reactive ion etching, laser trimming, embossing or through-mask UV irradiation of chelate modified gels and subsequent dissolution [13–16]. Alternatively, self-assembled monolayers have been used as ‘masks’ to direct formation of gel layers from precursor solutions [17–19]. All the aforementioned

methods, however, produce dispersed, non-percolating metal nanoclusters embedded in an insulating ceramic phase.

An interpenetrating network composite is one in which each constituent phase is continuous and interpenetrating throughout the microstructure [20]. Previous reports of interpenetrating network nanocomposites are largely limited to organic–organic [21] and organic–inorganic material systems [22]. Prior work in metal–ceramic material systems involves micrometre-scale phases and hence, by definition, may not be classified as nanocomposites [23]. Au–TiO₂ interpenetrating network nanocomposites are expected to have the functionalities of its constituents such as the wear resistance of TiO₂ together with the high electrical conductivity of Au [20]. Thin films of Au and its alloy have been widely used as contact material in micro-switch devices because of their low resistivity and oxidation resistance [24]. However, they suffer from wear and stiction, which shorten device lifetimes [25]. In contrast, TiO₂ films formed using sol–gel processes have excellent wear resistance [10]. Currently, there are no prior reports on the fabrication of patterned micrometre scale metal–TiO₂ interpenetrating network nanocomposites.

Here, we demonstrate a novel technique to form patterned features of an interpenetrating network nanocomposite of Au and nanostructured TiO₂ (NST) suitable for microsystem applications.

2. Experimental details

The technique developed for fabricating interpenetrating Au–NST network nanocomposites involves two main steps—firstly forming porous NST patterns, and secondly infiltrating NST patterns with Au using electroless deposition. A schematic diagram of the process is shown in figure 1. NST pad arrays with porous sponge-like morphology were formed by reacting patterned arrays of exposed Ti surfaces with aqueous hydrogen peroxide (aq. H₂O₂) solution followed by low temperature annealing. To prepare Ti thin film samples, 2.5 cm square pieces of either N-type Si(100) or glass pieces were used as substrates. Si pieces were first thermally oxidized at 1100 °C to grow a 1 μm thick silicon dioxide (SiO₂) layer. For glass substrates, a 1 μm thick SiO₂ layer was deposited by plasma-enhanced chemical vapour deposition (PECVD). Prior to the deposition of Ti films, substrates were cleaned with ultrasonic agitation for 5 min each in acetone, 2-propanol and de-ionized (DI) water (18.9 MΩ) and blown dry with nitrogen. Ti film was deposited on substrates by electron beam evaporation at a process pressure of $\sim 5.0 \times 10^{-7}$ Torr. Ti sources used were of 99.995% purity or better. After Ti deposition, a 1 μm thick SiO₂ layer was deposited using PECVD. The SiO₂ layer was then patterned using conventional photolithography followed by etching with CHF₃ gas to expose Ti patterns. The exposed patterns of Ti surfaces were oxidized by ageing in 10% (by volume) aq. H₂O₂ at 80 °C. This was followed by annealing at 300 °C for a few hours. Ageing and annealing steps were done in ambient air.

Au was infiltrated into pores of NST pads using electroless deposition. Commercially available electroless gold plating solution, based on alkaline gold cyanide complex with disodium ethylenediaminetetraacetate (Na₂EDTA) as chelating agent, was purchased in a ready to use condition. Plating was done by immersing samples in a heated bath of the plating solution. Prior to immersion, the temperature of the solution was maintained and stabilized at 60 ± 2 °C. For every Au deposition process, fresh plating solution was used to ensure similar Au deposition rate. After plating, samples were soaked and rinsed thoroughly in deionized water and subsequently blown dry with nitrogen. Although Au was used in this study, the process can be generalized to other metals that can be deposited using electroless deposition.

Various techniques were used to characterize the NST and Au–NST nanocomposites fabricated. Crystal structure was analysed by x-ray diffraction in Bragg–Brentano configuration using Cu Kα radiation (1.5406 Å) (Phillips X’pert-MPD). Structural characterization was done using an FEI dual-beam focus ion beam system equipped with Ga ion and electron columns for high resolution machining and imaging operations, respectively. Surface chemical species were determined using a Kratos Axis Ultra x-ray photoelectron spectroscopy (XPS) system. High resolution and survey XPS scans of various surfaces were performed. XPS spectra collected were fitted using commercial software

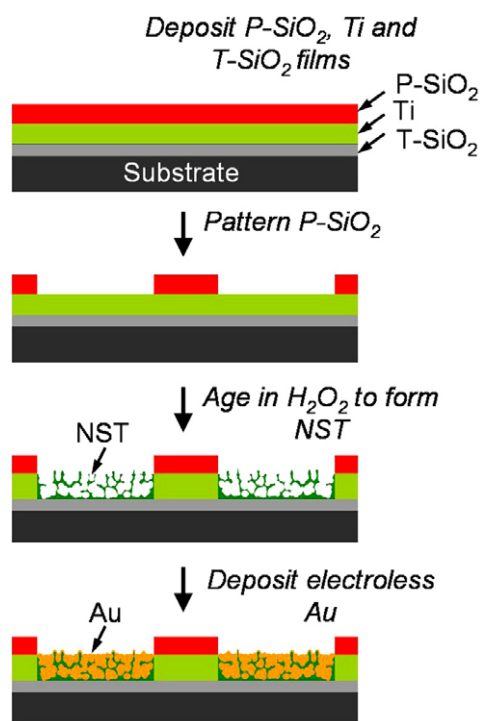


Figure 1. Schematic process flow for forming a patterned Au–NST nanocomposite. (T-SiO₂ and P-SiO₂ denote thermally grown SiO₂ and SiO₂ deposited by PECVD, respectively.)

(CasaXPS). Surface morphology of parent Ti, NST and Au–NST nanocomposite was investigated using tapping mode atomic force microscopy (AFM).

3. Results and discussion

The reaction of metallic Ti with hydrogen peroxide had been investigated previously and was shown to result in the formation of a hydrated TiO₂ gel layer [26]. TiO₂ layers formed using this technique are generally crack filled and not suitable for device applications [27, 28]. We have recently developed a technique that allows integration of crack-free NST features into microsystems. This method involves patterning Ti surfaces prior to reaction with hydrogen peroxide [28]. After ageing in hydrogen peroxide and subsequent annealing, NST patterns have a nanoporous sponge-like morphology with interconnecting pore walls.

3.1. Scanning electron microscopy studies

The typical morphology of NST formed is shown in figures 2(a)–(c). The pore walls have thickness ranging from about 75–125 nm while pore diameters range from 50 to 200 nm. Unannealed NST patterns are hydrated TiO₂ gels consisting of peroxo-compounds [26]. In some regions, walls of pores are long and narrow enough to be described as wires. The porous structure of NST could be due to morphology of the intermediate gel layer formed during ageing in aq. H₂O₂. It is suggested that porosity in the gel layer formed during aqueous oxidation is preserved when the gel is transformed to solid TiO₂ upon annealing. Similar porous microstructures were observed when unpatterned bulk Ti foil was reacted with aq. H₂O₂ [28]. Figure 2(c) is a cross-sectional SEM

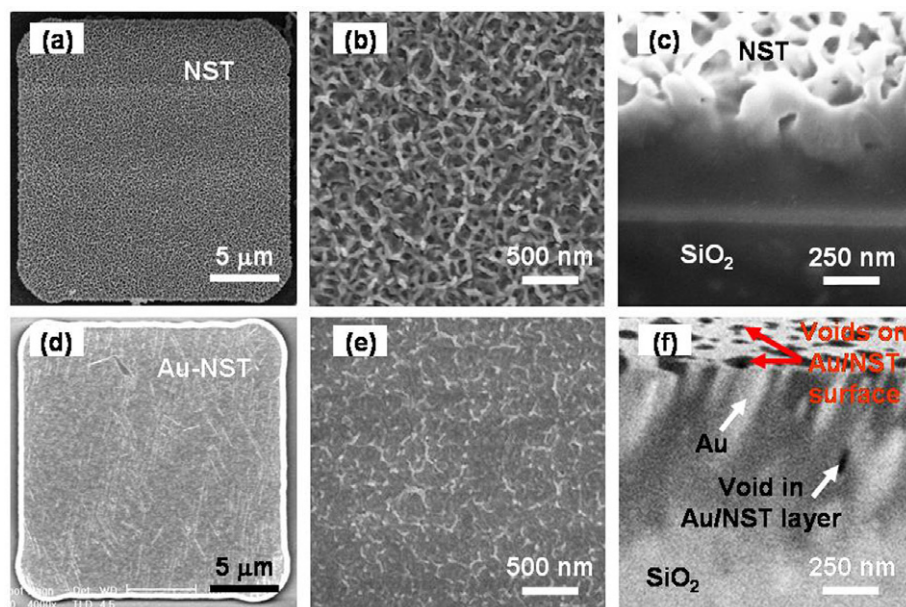


Figure 2. SEM images of NST: (a)–(c) before Au infiltration; (a) top view of a 20 μm pad; (b) higher magnification image; (c) cross-sectional images after micromachining (tilt 30°); (d)–(f) corresponding images after Au infiltration—the tilt in (f) is 52°. (The resolution of these images is ~ 1 nm.)

image of NST obtained after focus ion beam milling. The cross-sectional image reveals that the 350 nm thick Ti layer had been fully oxidized and the porous structure of the NST layer formed extends to the underlying SiO₂ surface. NST patterns formed have excellent adhesion to the underlying SiO₂. In contrast, NST formed from unpatterned Ti surfaces delaminates extensively [27, 28].

Figures 2(d)–(f) are typical SEM images of Au–NST nanocomposites formed after electroless deposition of Au on NST patterns. Protrusions 25–50 nm high decorated the surface of the Au–NST nanocomposites. These protrusions were formed when Au plates on TiO₂ walls that protrude from the NST layer. After infiltration, pores of the NST patterns were completely filled with Au. Figure 2(f), which is a cross-sectional image of the Au–NST nanocomposite, shows that Au has deposited in the pores throughout the NST pad and not only on the surface. No significant voids were evident in the Au–NST nanocomposites. However, holes with depths of about 30 nm were observed on the surface of nanocomposites. This suggests that during plating, there is no significant difference between the rate of Au deposition in the NST layers and that on the surface of these layers. This could be due to the relatively large pore size of the NST after annealing.

3.2. X-ray diffraction studies

Using x-ray diffraction studies in both Bragg–Brentano and pole figure geometries, we have previously reported in detail the phase evolution of NST after various process steps [28]. Here we provide only a brief description. We found that after ageing in aq. H₂O₂ NST consists, largely, of amorphous TiO₂ and nanocrystals of anatase and that the amorphous TiO₂ phase transforms to anatase upon annealing. Figure 3(a) shows XRD spectra of as-deposited Ti film, aged and annealed NST formed from evaporated unpatterned Ti film. In this sample, a thick Ti layer (about 2 μm) is partially oxidized in 10%

H₂O₂ solution for 2.5 h at 80 °C leaving a residual Ti layer to prevent complete delamination of the film. The sample is then subsequently annealed at 300 °C for 8 h. After ageing, three broad low intensity peaks at 2θ values of 25.20°, 47.97° and 62.68° were observed in addition to the Ti peaks from residual unreacted Ti layer. These three additional peaks can be assigned to {101}, {200} and {204} planes of anatase. The broadness and low intensity of these peaks suggest that as-formed NST consists of anatase nanocrystals in a largely amorphous matrix. These peaks sharpened and increase in intensity upon annealing. In addition, a second set of peaks at 53.91°, 54.95° and 75.04° appeared after the annealing step. These latter peaks correspond to {105}, {211} and {215} reflections of anatase. These observations are in agreement with previous reports [29, 30].

XRD studies of patterned, composite Au–NST pad arrays indicate that Au was deposited on NST pads only and not on the SiO₂ mask—see figure 3(b). Such selective deposition was observed on amorphous and crystalline NST. A comparison of XRD spectra of the sample after Au plating indicates the presence of three peaks at 2θ values of 44.18°, 64.46° and 81.76° on the NST pad array. The three peaks observed can be assigned to the {200}, {220} and {222} of Au. A prior study of electroless Au deposition on Ti films, which has an amorphous native oxide, has reported the presence of these three Au reflections [31]. These peaks, however, are not present in spectra collected from the SiO₂ mask region. These observations strongly indicate that Au has deposited only in pores of the NST pads and not on the surface of the SiO₂ mask. Ti peaks were observed in the XRD spectra because the samples used were only partially oxidized.

3.3. X-ray photoelectron spectroscopy studies

Results of XPS studies are shown in figures 4(a)–(d). All spectra were referenced to the C 1s peak at 285.0 eV. Figure 4(a)

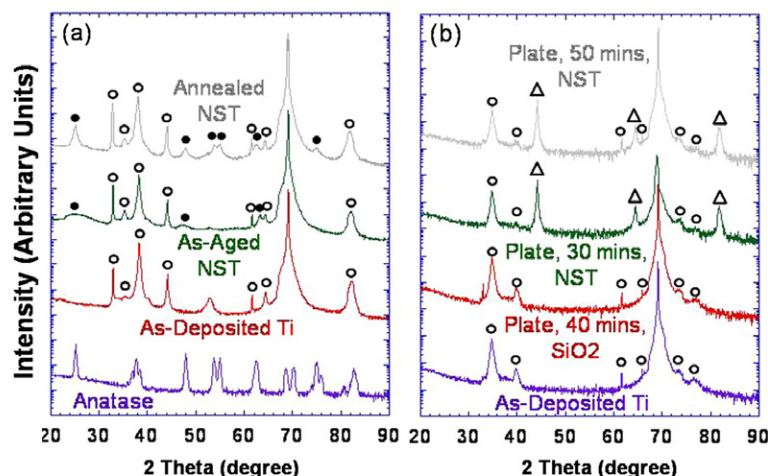


Figure 3. XRD of samples illustrating (a) NST phase evolution and (b) selective Au deposition on unannealed NST. (●—anatase TiO₂, ○—Ti and △—Au.)

is a high resolution scan of the Ti 2p peaks of unpatterned NST film formed on PECVD SiO₂ on Si substrate after annealing at 8 h for 300 °C. Similar results were obtained from NST formed on a PECVD SiO₂ coated glass substrate. Fitting of the raw XPS spectra was done using commercial XPS analysis software (CasaXPS). From the analysis, binding energies of Ti 2p_{3/2} and Ti 2p_{1/2} were found to be 458.9 and 464.8 eV, respectively. These values are close to those reported in the literature for TiO₂, at 458.9 and 464.6 eV for Ti 2p_{3/2} and Ti 2p_{1/2}, respectively, and confirm the formation of TiO₂ after annealing [32, 33].

Figure 4(b) shows XPS spectra of unpatterned NST film before and after 5 min Au plating. Before plating only Si 2p signal with a peak at 101.3 eV was detected. After plating, however, three additional peaks were detected. Two peaks at binding energies of 84.60 and 88.16 eV are assigned to Au 4f_{7/2} and Au 4f_{5/2}. These experimental values of Au 4f_{7/2} and Au 4f_{5/2} obtained are consistently higher than, by 0.38 and 0.22 eV respectively, but close to the corresponding values reported in the literature, which range from 83.70 to 84.25 eV for Au 4f_{7/2} and 87.71 to 87.94 eV for Au 4f_{5/2} of Au [34–36]. The peak at 63.13 eV in figure 4(b) is assigned to Na 2s; another peak, which is assigned to Na 1s, at 1071.58 eV was also observed after plating. It is known that Na when dissolved in Au, may exist as Au(Na) alloy and/or Au_nNa (where $n = 5, 2, 1$) intermetallic compounds [37]. Solomun had determined Na 1s binding energies of a superficial Au(Na) alloy to be about 1071.05 eV, which is close to that obtained in the present study [38]. The similarity in binding energies suggests formation of a dilute Au(Na) alloy in the present study. During plating some Na ions are entrapped and incorporated in the Au lattice, resulting in formation of a Au(Na) alloy. Incorporation of Na ions in Pd layers during electroless deposition from a plating bath that similarly used Na₂EDTA chelating agent had been reported previously [39]. Unfortunately there are no reports in the literature of Au 4f_{7/2} and Au 4f_{5/2} binding energies from Au_nNa intermetallic compounds for comparison. However, the presence of Au_nNa compounds after plating, if any, is not extensive because no XRD reflections detected can be assigned to these compounds.

From the preceding discussion it may be concluded that Na was incorporated into Au during plating.

Results of area-mode XPS studies confirm Au deposits selectively on NST. Figures 4(c) and (d) show Si 2p and Au 4f signals, respectively, of an arbitrary region of the NST pad array after electroless Au plating. Results of area-mode XPS are presented in a grey scale where areas with higher concentration of a chemical species appear brighter. Since XPS is a technique sensitive to chemical species from the first few nanometres of the surface only [40], the strong Si 2p signal indicates that very little, if any, Au has deposited on the SiO₂ mask oxide. This is confirmed in figure 4(d) that shows Au 4f signal only in areas corresponding to those of NST pads. Therefore, XPS results are in agreement with those of XRD studies and strongly indicate Au has been deposited selectively on NST features.

3.4. Atomic force microscopy studies

Surface morphologies of the parent Ti thin film, NST and Au–NST nanocomposite formed were studied using atomic force microscopy (AFM). Figures 5(a)–(c) show typical images of these surfaces. The surface of the parent Ti film is rough, consisting of distinctly faceted Ti nanocrystals separated by gaps. Ti crystals are platelet-like with thickness and longest width of 40 ± 10 nm and 124 ± 31 nm, respectively. (All stated dimensions are an average and one standard deviation of 30 measurements.) In some regions of the Ti surface, gaps are large enough to be described as troughs with average diameter of about 101 ± 37 nm. AFM images of surfaces of NST formed after oxidation and subsequent annealing steps show a distinctly different morphology from that of the as-deposited Ti. The NST surface is rough with ridge-like protrusions that surround holes. The ridges correspond to TiO₂ walls and consist of spherical protrusions about 93 ± 32 nm in diameter. The average diameter of holes was measured to be about 126 ± 33 nm. After Au plating, the surface of the Au–NST nanocomposite consists of globular grains with average diameter of about 52 ± 12 nm. This results in a smoother surface, as Au was deposited in the troughs and on the walls of the NST layer.

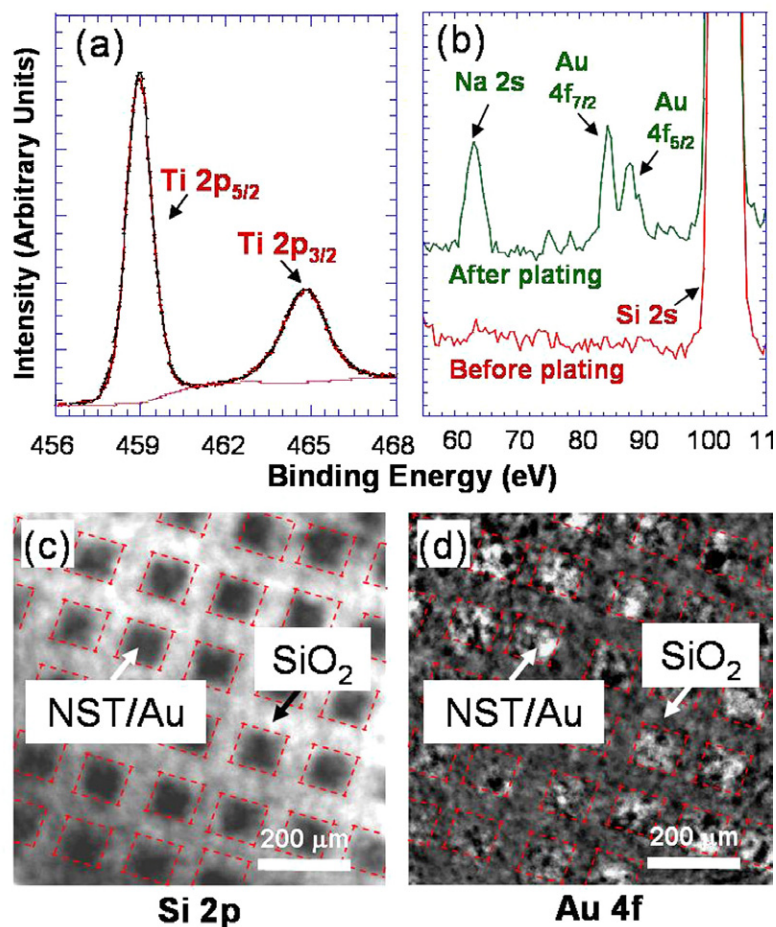


Figure 4. XPS results of (a) Ti 2p high resolution line scans of NST before Au plating and (b) line scans before and after Au plating for binding energies from 55 to 110 eV. XPS area scans of (c) Si 2p and (d) Au 4f, both after Au plating.

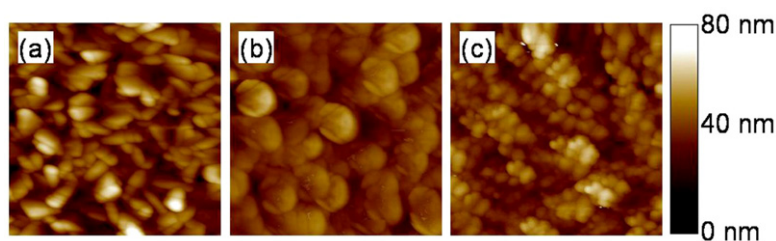


Figure 5. Two-dimensional AFM images of (a) as-deposited Ti film, (b) as-formed NST and (c) Au–NST nanocomposite formed after Au plating. (Dimensions of images are $1 \times 1 \mu\text{m}^2$.)

4. Conclusions

In conclusion, a two-step process was developed for fabricating integrated and patterned micrometre-scale features of interpenetrating Au–nanostructured TiO₂ (NST) network nanocomposites. The process consists of, firstly, forming porous NST patterns and, secondly, infiltrating NST patterns with Au using electroless deposition. The following was found.

- As-aged NST is largely amorphous but transforms to single-phase anatase upon annealing.
- Although holes were found on the surface of Au–NST nanocomposite, no significant void formation in these layers was observed.

(c) Au was deposited selectively on NST pads and not on the SiO₂ mask.

Although Au has been used in this study, other metals that can be deposited using electroless deposition would work just as well. Hence this technique is a general route for forming integrated patterns of interpenetrating metal–NST network nanocomposites in microsystems.

Acknowledgments

The authors acknowledge support for this work from the Microsystems Technology Office of the Defence Advanced Research Projects Agency. This work made use of MRL

Central Facilities supported by the MRSEC Programme of the National Science Foundation under award No DMR-00-80034. ASZ acknowledges the International Fellowship (National Science Scholars Programme) from the Agency for Science, Technology and Research, Singapore, and Professor David R Clarke for helpful discussions regarding developments in bulk interpenetrating network composites.

References

- [1] Roy R, Roy R A and Roy D M 1986 *Mater. Lett.* **4** 323
- [2] Seal S and Baraton M-I 2004 *MRS Bull.* **29** 9
- [3] Zhang Q F, Liu W M, Xue Z Q, Wu J L, Wang S F, Wang D L and Gong Q H 2003 *Appl. Phys. Lett.* **82** 958
- [4] Bowker M, Stone P, Bennett R and Perkins N 2002 *Surf. Sci.* **497** 155
- [5] Liao H B, Xiao R F, Wang H, Wong K S and Wong G K L 1998 *Appl. Phys. Lett.* **72** 1817
- [6] Chen C C, Hashimoto M, Shi J, Nakamura Y, Nittono O and Barna P B 2003 *J. Appl. Phys.* **93** 6273
- [7] Casula M F, Corrias A, Falqui A, Serin V, Gatteschi D, Sangregorio C, Fernandez C D and Battaglin G 2003 *Chem. Mater.* **15** 2201
- [8] Takahashi R, Sato S, Sodesawa T, Nakamura N, Tomiyama S, Kosugi T and Yoshida S 2001 *J. Nanosci. Nanotechnol.* **1** 169
- [9] Epifani M, Giannini C, Tapfer L and Vasanelli L 2000 *J. Am. Ceram. Soc.* **83** 2385
- [10] Zhang W G, Liu W M, Li B and Mai G X 2002 *J. Am. Ceram. Soc.* **85** 1770
- [11] Livage J 1997 *Curr. Opin. Solid State Mater. Sci.* **2** 132
- [12] Hench L L and West J K 1990 *Chem. Rev.* **90** 33
- [13] Holmes A S, Syms R R A, Li M and Green M 1993 *Appl. Opt.* **32** 4916
- [14] Brylewski T and Przybylski K 1993 *Appl. Supercond.* **1** 737
- [15] Krug H, Merl N and Schmidt H 1992 *J. Non-Cryst. Solids* **147** 447
- [16] Tada H, Hattori A, Tokihisa Y, Imai K, Tohge N and Ito S 2000 *J. Phys. Chem. B* **104** 4585
- [17] Jeon N L, Clem P G, Nuzzo R G and Payne D A 1995 *J. Mater. Res.* **10** 2996
- [18] Kim E, Whitesides G M, Lee L K, Smith S P and Prentiss M 1996 *Adv. Mater.* **8** 139
- [19] Collins R J, Shin H, DeGuire M R, Heuer A H and Sukenik C N 1996 *Appl. Phys. Lett.* **69** 860
- [20] Clarke D R 1992 *J. Am. Ceram. Soc.* **75** 739
- [21] Decker C 2002 *Macromol. Rapid Commun.* **23** 1067
- [22] Sharp K G 1998 *Adv. Mater.* **10** 1243
- [23] Breslin M C, Ringnalda J, Xu L, Fuller M, Seeger J, Daehn G S, Otani T and Fraser T L 1995 *Mater. Sci. Eng. A* **195** 113
- [24] Hyman D and Mehregany M 1999 *IEEE Trans. Compon. Packag. Technol.* **22** 357
- [25] Coutu J R, Kladitis P E, Leedy K D and Crane R L 2004 *J. Micromech. Microeng.* **14** 1157
- [26] Tengvall P, Lundstrom I, Sjoqvist L, Elwing H and Bjurstein L M 1989 *Biomaterials* **10** 166
- [27] Wu J M, Hayakawa S, Tsuru K and Osaka A 2002 *Scr. Mater.* **46** 101
- [28] Zuruzi A S and MacDonald N C 2005 *Adv. Funct. Mater.* **15** 396
- [29] Zhang H Z, Finnegan M and Banfield J F 2001 *Nano Lett.* **1** 81
- [30] Chu S Z, Wada K, Inoue S and Todoroki S 2002 *Chem. Mater.* **14** 266
- [31] Hou Z Z, Abbott N L and Stroeve P 1998 *Langmuir* **14** 3287
- [32] Choudhury T, Saied S O, Sullivan J L and Abbott A M 1989 *J. Phys. D: Appl. Phys.* **11** 1185
- [33] Gonbeau D, Guimon C, Pfisterguillouzo G, Levasseur A, Meunier G and Dormoy R 1991 *Surf. Sci.* **254** 81
- [34] Fuggle J C, Kallne E, Watson L M and Fabian D J 1977 *Phys. Rev. B* **16** 750
- [35] Turner N H and Single A M 1990 *Surf. Interface Anal.* **15** 215
- [36] Thomas T D and Weightman P 1986 *Phys. Rev. B* **33** 5406
- [37] Massalski T B, Murray J L, Bennett L H and Baker H (ed) 1986 *Binary Alloy Phase Diagrams* (Metals Park, OH: American Society for Metals)
- [38] Solomun T 1995 *Surf. Sci.* **331–333** 52
- [39] Chen H-I, Hsiung C-K and Chou Y-I 2003 *Semicond. Sci. Technol.* **18** 620
- [40] Moulder J F, Stickle W F, Sobol P E and Bomben K D 1995 *Handbook of X-Ray Photoelectron Spectroscopy: A Reference Book of Standard Spectra for Identification and Interpretation of XPS Data* (Minnesota: Physical Electronics Inc.)